

Article

# Incorporation of Ca, P, Mg, and Zn Elements in Ti-30Nb-5Mo Alloy by Micro-Arc Oxidation for Biomedical Implant Applications: Surface Characterization, Cellular Growth, and Microorganisms' Activity

Giovana Collombaro Cardoso <sup>1,2,\*</sup>, Katia Barbaro <sup>3</sup> , Pedro Akira Bazaglia Kuroda <sup>1</sup>, Luca Imperatori <sup>2</sup>, Angela De Bonis <sup>4</sup> , Roberto Teghil <sup>4</sup> , Mariangela Curcio <sup>4</sup> , Elisa Innocenzi <sup>3</sup>, Victoria Yu. Grigorieva <sup>5</sup> , Gianluca Vadalà <sup>6,7</sup>, Carlos Roberto Grandini <sup>1</sup>  and Julietta V. Rau <sup>2,5</sup> 

- <sup>1</sup> Laboratório de Anelasticidade e Biomateriais, UNESP—Universidade Estadual Paulista, Bauru 17033-360, SP, Brazil; pedro.kuroda@unesp.br (P.A.B.K.); carlos.r.grandini@unesp.br (C.R.G.)
- <sup>2</sup> Istituto di Struttura della Materia, Consiglio Nazionale delle Ricerche (ISM-CNR), Via del Fosso del Cavaliere 100, 00133 Rome, Italy; luca.imperatori@cnr.it (L.I.); giulietta.rau@ism.cnr.it (J.V.R.)
- <sup>3</sup> Istituto Zooprofilattico Sperimentale Lazio e Toscana “M. Aleandri”, Via Appia Nuova 1411, 00178 Rome, Italy; katia.barbaro@izslt.it (K.B.); elisa.innocenzi-esterno@izslt.it (E.I.)
- <sup>4</sup> Dipartimento di Scienze, Università della Basilicata, Via dell’Ateneo Lucano 10, 85100 Potenza, Italy; angela.debonis@unibas.it (A.D.B.); roberto.teghil@unibas.it (R.T.); mariangela.curcio@unibas.it (M.C.)
- <sup>5</sup> Department of Analytical, Physical and Colloid Chemistry, Institute of Pharmacy, Sechenov First Moscow State Medical University, Trubetskaya 8, Build. 2, 119991 Moscow, Russia; grigoreva\_v\_yu@staff.sechenov.ru
- <sup>6</sup> Laboratory of Regenerative Orthopaedics, Research Unit of Orthopaedic, Department of Medicine and Surgery, Università Campus Bio-Medico di Roma, Via Alvaro del Portillo 21, 00128 Rome, Italy; g.vadala@policlinicocampus.it
- <sup>7</sup> Operative Research Unit of Orthopaedics, Fondazione Policlinico Universitario Campus Bio-Medico, Via Alvaro del Portillo 200, 00128 Rome, Italy
- \* Correspondence: giovana.collombaro@unesp.br



**Citation:** Cardoso, G.C.; Barbaro, K.; Kuroda, P.A.B.; Imperatori, L.; De Bonis, A.; Teghil, R.; Curcio, M.; Innocenzi, E.; Grigorieva, V.Y.; Vadalà, G.; et al. Incorporation of Ca, P, Mg, and Zn Elements in Ti-30Nb-5Mo Alloy by Micro-Arc Oxidation for Biomedical Implant Applications: Surface Characterization, Cellular Growth, and Microorganisms' Activity. *Coatings* **2023**, *13*, 1577. <https://doi.org/10.3390/coatings13091577>

Academic Editors: Anita Ioana Visan and Gianina Popescu-Pelin

Received: 5 August 2023

Revised: 4 September 2023

Accepted: 7 September 2023

Published: 10 September 2023



**Copyright:** © 2023 by the authors. Licensee MDPI, Basel, Switzerland. This article is an open access article distributed under the terms and conditions of the Creative Commons Attribution (CC BY) license (<https://creativecommons.org/licenses/by/4.0/>).

**Abstract:** Micro-arc oxidation (MAO) is a surface modification technique used to improve the surface properties of titanium alloys, such as corrosion, wear resistance, and osseointegration. In addition to promoting the growth of a porous oxide coating on the sample's surface, it is also possible to incorporate bioactive elements into this coating, such as calcium, phosphorus, and magnesium, as well as elements with antimicrobial action, such as zinc. Thus, this study aimed at the surface modification of the  $\beta$  Ti-30Nb-5Mo alloy by the MAO method, incorporating calcium, phosphorus, magnesium, and zinc to improve osseointegration and promote bactericidal character in the produced coating. The results showed that the porosity, roughness, and crystallinity of the coating tend to increase with increasing Zn concentration in the electrolyte, while the contact angle decreases. The antimicrobial activity was promoted against the *E. faecalis* and *P. aeruginosa* bacteria strains and the *C. albicans* fungus. Incorporating Zn on the surface also did not negatively affect adiposetissue-derived mesenchymal stem cell differentiation, and promoted more significant growth of these cells on the samples' surface.

**Keywords:** antimicrobial activity; micro-arc oxidation; surface modification; titanium alloy; Ti-30Nb-5Mo alloy; zinc

## 1. Introduction

Titanium (Ti) and its alloys are widely used for biomedical applications, mainly in implants, due to their excellent properties, such as corrosion, wear resistance, and acceptable biocompatibility [1]. Compared to other metallic biomaterials, Ti also possesses osseointegration characteristics. That is, it can form a direct interface between the implant and the native bone without ligament or cartilage fibers [2]. However, this capability is

limited and may not be enough to prevent implant failures [1]. Furthermore, due to its artificial nature and lack of some bio-functional properties, many clinical problems still occur during Ti implant application, such as material fracture, stress shielding, cytotoxicity, corrosion, and infections [1–3].

Among these and other problems, infections deserve attention, as the implant is a foreign body that increases the risk of propagation and invasion of bacteria in an organism that has low resistance due to the secondary surgeries in order to replace this material [4]. Between 50 to 70% of hospital infections come from internal medical devices [5,6], and when talking about infections from orthopedic surgeries, the risk is from 2 to 5% [5]. The *S. aureus* bacteria strain is common in nosocomial infections, and it is estimated that approximately 34% of orthopedic implant infections are caused by it. The *E. coli* bacteria strain, on the other hand, has several adhesion mechanisms that make it capable of adhering to materials and instruments used in hospitals [6]. A further complication of the situation is due to conventional antibiotics that are often not efficient during treatment, leading to the need to remove the implant, causing stress, discomfort, and pain to the patient, and additional costs for healthcare. It is estimated that biofilms can develop resistance against antibiotics from 10 to 1000 times [7]. Therefore, studies seeking to prevent and control infections caused by implants are increasing [1,8].

It is known that some of the excellent properties of Ti and its alloys are due to the amorphous layer, on a micrometric or nanometric scale, of titanium oxide (TiO<sub>2</sub>) formed on its surface, which grows spontaneously soon after implantation [2,9]. Thus, the treatments and functionalization of Ti alloys' surfaces are utilized to add bio-functional properties to the material. There are many techniques for modifying the surface of Ti alloys, such as sol-gel, sputtering, and anodization. However, there are some disadvantages in using these methods, such as the high cost of the sol-gel technique [10], and the difficulty of obtaining an adherent coating when high loads are applied to the implant that was treated using sputtering [11] or anodization [12] techniques.

Micro-arc oxidation (MAO) is a simple and inexpensive method, producing surfaces with high corrosion and wear resistance [13,14] and mechanical strength [15,16]. After surface treatment by MAO, the sample can still increase its adhesion and cell proliferation, depending on the electrolyte solution and oxidation time [17–19]. Different alloying elements can also influence the coating's morphology, microstructure, and mechanical properties [19,20]. The MAO technique can easily incorporate bactericidal particles into the produced coating [2], supplying additional bio-functionality to the Ti alloy.

Calcium (Ca), phosphorus (P), and magnesium (Mg) ions, for example, can also be added to the surface of micro-arc oxidized alloys, improving their osseointegration properties [21], wear resistance, and tribocorrosion [22]. Silver (Ag) and copper (Cu) are examples of elements that improve the bactericidal activity of the surfaces treated with MAO when added to the electrolytic solution [23–27]. However, there is some concern with using these elements, since their high concentrations in the human body can be harmful [28,29]. In addition to Ag and Cu, Zinc (Zn) is also used as a bactericidal agent [30,31]. Although it has lower efficiency and a cytotoxic character in high amounts [28,32], low concentrations of this element on the surface oxidized by MAO can promote cell adhesion, proliferation, and differentiation, according to Zhu et al. [33]. This is because the presence of Zn can influence the enzymes that participate in the synthesis of various components of the bone matrix. In addition, Zn is a crucial microelement of the human body that participates in several biological processes, such as enzyme activity, DNA synthesis, biomineralization, and acid metabolism [4,34].

The Ti-30Nb-5Mo alloy is a recently developed  $\beta$  alloy that has a low elastic modulus and hardness (but still high enough to have better wear resistance than Commercially Pure (CP)-Ti), in addition to promoting cell adhesion and proliferation without cytotoxicity [35–37]. Furthermore, niobium (Nb) is already known in the biomedical field for its ability to increase the corrosion resistance of Ti alloys [38,39]. Since it is a new alloy, no other literature references report on its surface modification.

Thus, the objective of this paper was to perform surface treatment of the Ti-30Nb-5Mo alloy using the MAO technique, in order to develop coatings containing Ca, P, and Mg, and to vary the Zn concentration in the electrolytic solution. In addition, the purpose was to evaluate the influence of Zn on cell and microorganism growth on the treated Ti alloy surface.

## 2. Materials and Methods

The Ti-30Nb-5Mo alloy was produced by arc-melting in an argon-controlled atmosphere and in a water-cooled copper crucible. The details of the cast and bulk properties of this alloy can be found in previous works [35–37]. After melting, the produced ingots were hot rolled to reach a thickness of 1 mm, and cut to obtain square samples measuring  $10 \times 10 \text{ mm}^2$ . Finally, the samples were heat-treated for 6 h, at  $1000 \text{ }^\circ\text{C}$ , with heating and cooling rates of  $10 \text{ }^\circ\text{C}/\text{min}$ .

MAO treatments were performed using a DC power source Keysight, N5751A (Keysight, Santa Rosa, CA, USA), with limited current of 2.5 A, 300 V, at room temperature, for 60 s. At first, a solution of 0.35 M calcium acetate monohydrate ( $(\text{CH}_3\text{COO})_2\text{Ca}\cdot\text{H}_2\text{O}$ ), 0.02 M  $\beta$ -glycerol phosphate pentahydrate ( $\text{C}_3\text{H}_7\text{Na}_2\text{O}_6\text{P}\cdot 5\text{H}_2\text{O}$ ), and 0.1 M magnesium acetate tetrahydrate ( $(\text{CH}_3\text{COO})_2\text{Mg}\cdot 4\text{H}_2\text{O}$ ) was used as the electrolyte to produce the samples without Zn particles (0.0 Zn). To obtain the surface samples with Zn, the same solution was used with the addition of 0.5 mMol (0.5 Zn), 1.0 mMol (1.0 Zn), or 2.5 mMol (2.5 Zn) zinc chloride ( $\text{ZnCl}_2$ ). Table 1 shows a summary of the electrolyte solution used for each sample.

**Table 1.** Summary of the sample labels and electrolyte solution composition used during the MAO treatments.

Sample Label	Calcium Acetate (mol/L)	$\beta$ -Glycerol Phosphate (mol/L)	Magnesium Acetate (mol/L)	Zinc Chloride (mmol/L)
#0	-	-	-	-
0.0 Zn	0.35	0.02	0.1	-
0.5 Zn	0.35	0.02	0.1	0.5
1.0 Zn	0.35	0.02	0.1	1.0
2.5 Zn	0.35	0.02	0.1	2.5

SEM images were obtained using a Zeiss scanning electron microscope (Carl Zeiss, Oberkochen, Germany), model 300 FE. Information of porosity and pore size was obtained from micrographs with the ImageJ software (version 1.53t) by analyzing eight regions on each sample's surface, with different dimensions (ranging from 350 to  $1200 \mu\text{m}^2$ ). The result was presented as the mean and standard deviation of the measurements. Regarding the pore size, this measurement represents the size of pores within each selected area.

XRD results were obtained by a MiniFlex600 diffractometer (Rigaku, Tokyo, Japan) with  $\text{Cu K}\alpha$  radiation ( $\lambda = 1.54056 \text{ \AA}$ ) ranging from  $10^\circ$  to  $100^\circ$ , with steps of  $0.04^\circ$  and  $10^\circ/\text{min}$  collection time.

XPS spectra were acquired by a SPECS Phoibos 100-MCD5 spectrometer (SPECS Berlin, Berlin, Germany) equipped with a  $\text{AlK}\alpha$  (1486.6 eV) achromatic radiation source, operating at 100 W in FAT mode. Channel widths of 1 and 0.1 eV were used for wide and detailed regions, respectively.

Information about the wettability of the samples was obtained using contact angle measurements by the droplet technique on a Krüss DSHAT HTM Reetz GmbH goniometer (HTM Reetz GmbH, Berlin, Germany). Deionized water was used to test the fluid in three different regions of the sample to calculate the mean and standard deviation.

AFM imagers were registered by a Park XE-120 microscope (Park, Suwon, Republic of Korea) operating in non-contact mode. Two  $30 \times 30 \mu\text{m}$  images were acquired to evaluate the surface roughness.

Bactericidal growth data on the Ti-30Nb-5Mo alloy substrate and coatings were obtained using four bacteria strains (*E. coli*, *S. aureus*, *E. faecalis*, and *P. aeruginosa*) and one

fungus (*C. albicans*). Before testing, all the samples were autoclaved at 121 °C for 20 min. Afterward, each sample was placed in tubes containing a suspension of a single microorganism in 5 mL of Brain Heart Infusion (BHI, DIFCO, Sparks, MD, USA). All assays were performed in triplicate to calculate mean and standard deviation, and tests performed only in BHI medium, without the presence of any sample, were used as control. Each microorganism was cultivated at its optimal growth temperature (37 °C for bacteria and 28 °C for fungus), with slow agitation, for 24 h. The growth of microorganisms was measured by reading the optical density at a wavelength of 600 nm (OD600) using a biophotometer (Eppendorf, Hamburg, Germany). The results were expressed in growth percentage with respect to the average OD600 of the microbial suspension without the samples.

MTT and differentiation tests were carried out using Adipose Mesenchymal Stem Cells (AMSC), which were isolated from the adipose tissue of three-month-old female lambs taken at the slaughterhouse. All assays were performed in triplicate to calculate mean and standard deviation, and, for positive control, the tests were performed by growing the AMSCs without the presence of any sample. After 24 h of incubation of the cells and substrates, the culture medium was removed, and 3 mL/well of a MTT solution (3-[4,5-dimethylthiazol-2-yl]-2,5-diphenyl-tetrazolium bromide, Sigma-Aldrich, Gillingham UK) was added to the DMEM medium (Gibco, Loughborough, UK) containing 10% FCS (Fetal Calf Serum, Gibco, Loughborough, UK), and incubated for 3 h at 37 °C with 5% CO<sub>2</sub>. After that, the MTT solution was replaced by 3 mL of absolute ethanol (Sigma-Aldrich, Gillingham, UK), and the solubilized formazan was measured by a biophotometer (Eppendorf, Hamburg, Germany) at 600 nm.

For osteogenic differentiation, AMSCs were treated for 3 weeks with DMEM medium containing 10% FCS supplemented with 50 µg/mL ascorbic acid, 10 mM β-glycerophosphate, and 10<sup>-7</sup> M dexamethasone. After that, the AMSCs were fixed in 70% ethanol for 1 h at room temperature, then washed with distilled water and stained for 30 min with 2% Alizarin Red S (Carlo Erba, Cornaredo, Italy) to detect the calcium deposits that, after four washes, turned orange-red.

The OriginPro2018 software was used for statistical analysis. The independent Two-Sample *t*-test analysis was used to estimate the difference between two population means. The results were classified and presented according to the significance level ( $p < 0.05$ ,  $p < 0.01$ , or  $p < 0.001$ ).

### 3. Results

#### 3.1. Surface Morphology

Micrographs of the surfaces after the MAO treatment are presented in Figure 1. All the samples' surfaces showed a typical morphology usually obtained by the MAO oxidation, composed of pores of different sizes. Pores of 0.1 µm diameter can be seen in the 0.0 Zn image at 10k× magnification (Figure 1b—yellow arrow). On surfaces with the incorporation of Zn, cracks appeared at the highest concentration of this element. In the images at high magnification, smaller pores inside the larger pore cavities were observed. Agglomerates of micrometric particles of the introduced elements were observed on all the surfaces of the Zn-containing samples, which were not detected on the sample's surface oxidized with the electrolyte containing only Ca, P, and Mg. Roknian et al. [40] studied the addition of ZnO particles on the surface of CP-Ti samples by the MAO method. They observed a similar effect of particle agglomerates on the surfaces containing Zn. During the MAO surface oxidation process, micro-arc discharges occur due to the dielectric breakdown of the anodic oxide coating [41]. As a result, a significant amount of heat is released, increasing the temperature [41,42]. However, the energy, and consequently the temperature of the process, was not high enough and, therefore, the Zn particles remained chemically unchanged, agglomerating on the sample's surface [41]. Other studies [39–41] also identified particle agglomerates on the surface of Ti alloys oxidized by micro-arc using an electrolytic solution containing Zn.

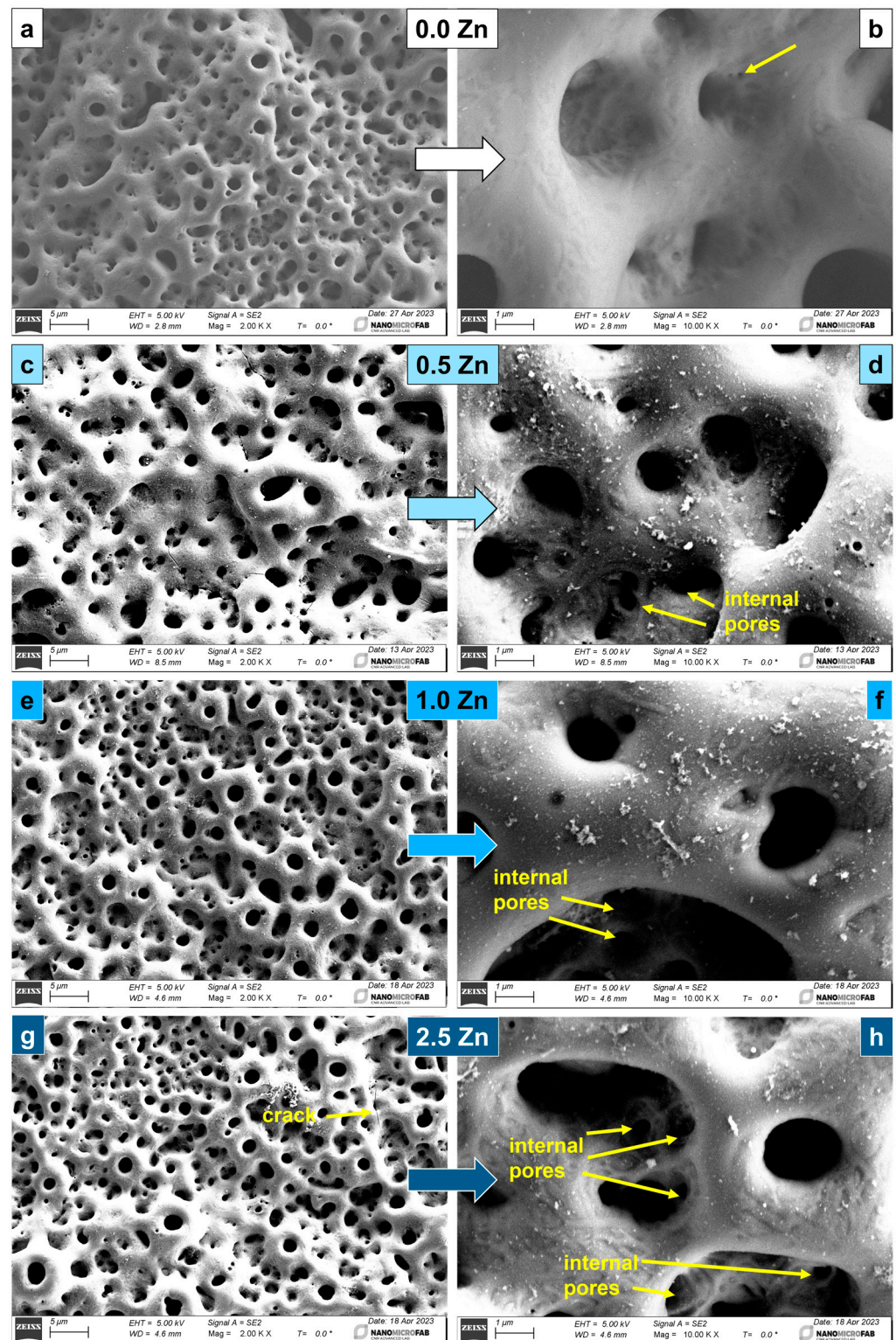


**Figure 1.** SEM images of 0.0 Zn (a,b), 0.5 Zn (c,d), 1.0 Zn (e,f), and 2.5 Zn (g,h) samples' surfaces after MAO treatment. Images (a,c,e,g) correspond to 2k $\times$  magnification, and (b,d,f,h) to 10k $\times$  magnification.

Histograms of the pore area produced on the surface of the samples are presented in Figure 2. The Zn variation was not enough to significantly change the pore size, and the largest number of pores had an area size of up to 0.05  $\mu\text{m}^2$ . With the data obtained by the histograms on the pore size of the coatings, it was possible to prepare the graph in Figure 3, which shows the relationship between the (s/T) ratio and the variation in the amount of

Zn in the MAO electrolytic solution. The (s/T) ratio is calculated by dividing the number of smaller pores (up to  $0.25 \mu\text{m}^2$ ) by the total number of measured pores. Thus, it was possible to better analyze the variation in the relative size of the pores produced on the samples' surface, since the higher the s/T is, the smaller the pores are. The addition of Zn increased the s/T ratio. This means that the number of smaller pores increased compared to the total number of the measured pores. For the 1.0 Zn sample, the number of small pores was even higher. However, for the 2.5 Zn sample, this ratio was again similar than that of the 0.5 Zn sample.

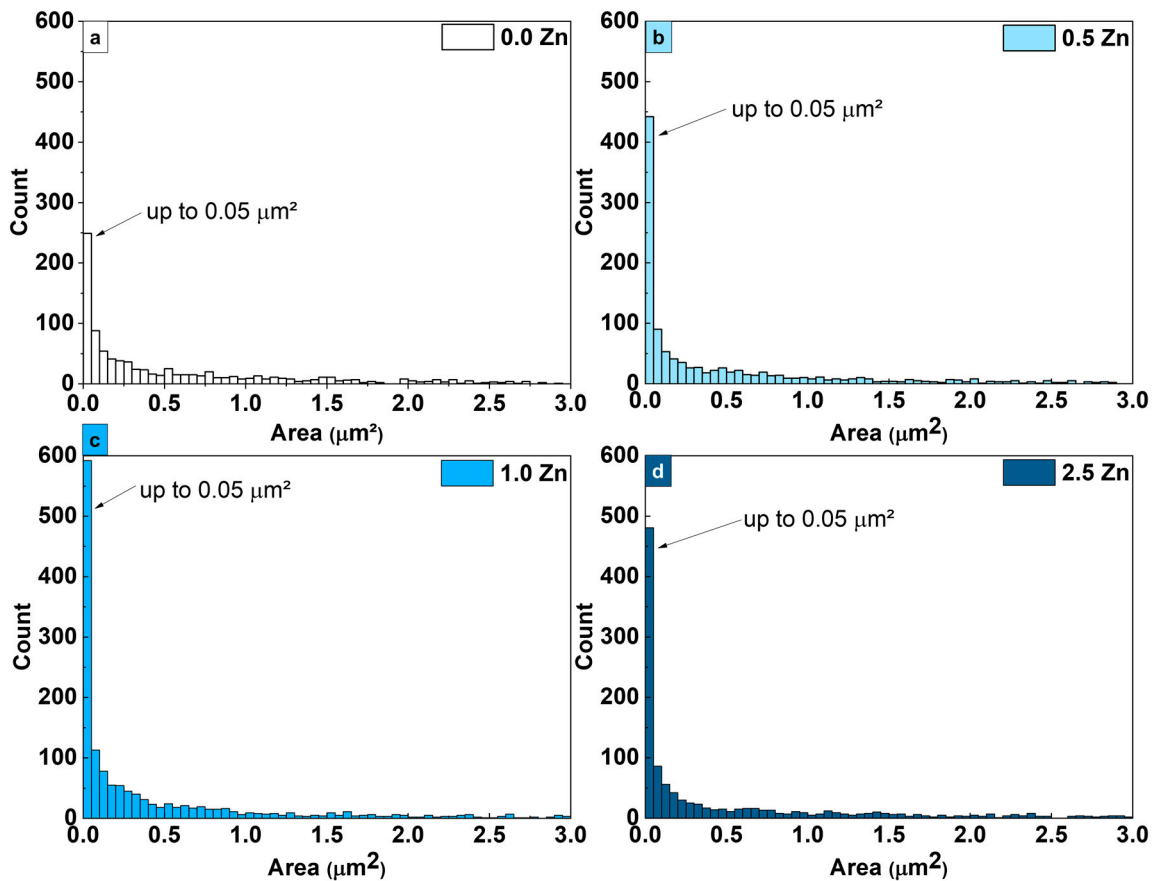


Figure 2. Pore area histogram of 0.0 Zn (a), 0.5 Zn (b), 1.0 Zn (c), and 2.5 Zn (d) samples.

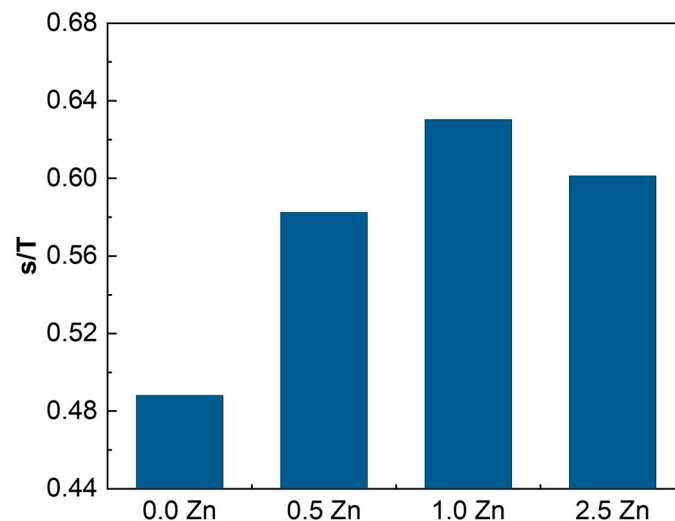


Figure 3. Relative pore size of the MAO coatings.

Figure 4 shows the porosity of the samples oxidized by MAO. The porosity of the 0.5 Zn sample does not suffer much variation with respect to the 0.0 Zn sample ( $p > 0.05$ ) due to the low concentration of Zn. Considering the samples with Zn, the porosity varies inversely to the s/T variation, since when the pores are larger (s/T smaller), the area occupied by the pores increased. The decrease in the pores' relative size and, consequently, the significant decrease ( $p < 0.05$ ) in the porosity of the 1.0 Zn sample may be related to the closing of the pores due to particles accumulating on the sample's surface [40], as can be seen in Figure 1. However, the porosity increased significantly again ( $p < 0.001$ ) in the 2.5 Zn sample, despite the pores closing due to the increase in the number of metallic ions in the electrolyte solution, which raised the conductivity of the medium and, consequently, increased the energy during oxidation. As a result, the quantity and size of the bubbles produced in the liquid increased, forming a surface with higher porosity [43].

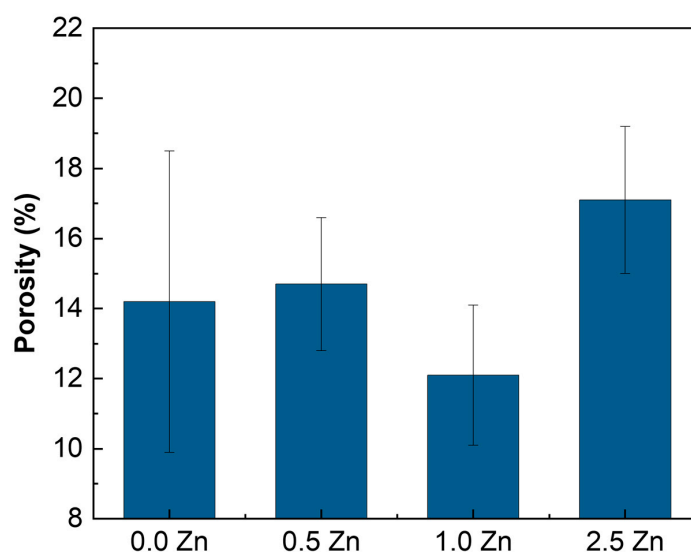


Figure 4. Porosity of the MAO coatings.

### 3.2. Structural Characterization

The XRD patterns of the samples are presented in Figure 5. In the Ti-30Nb-5Mo substrate, only characteristic peaks of the body-centered cubic (bcc) structure, known as  $\beta$ -Ti, were found [37]. This occurred due to the Nb and Mo, which are  $\beta$ -stabilizing elements. A  $\beta$ -stabilizing element has the characteristic of decreasing the Ti allotropic transformation temperature ( $\beta$ -transus), where its crystalline structure transforms from the  $\alpha$ -phase (hexagonal closest-packet—hcp) to the  $\beta$ -phase [44]. Upon undergoing MAO treatments, peaks indicating the presence of TiO<sub>2</sub> anatase and rutile phases were detected. As the amount of Zn increased in the electrolyte, other oxides were identified in the diffractograms: calcium phosphate (Ca(PO<sub>3</sub>)<sub>2</sub>) was detected in the 0.5 Zn, 1.0 Zn, and 2.5 Zn samples, while calcium oxide (CaO), and zinc oxide (ZnO) were found in the 1.0 Zn and 2.5 Zn samples. It was observed that the increase of Zn in the electrolyte favored the incorporation of the elements in the produced surface. This occurs because the increase in ions facilitated the transport of electrons in the sample, leading to a greater flow of elements from the liquid to the treated surface.

From the XRD data, the amount of oxide phase and surface crystallinity variation was calculated, and the results are shown in Figure 6. It is known that the activation energy required for the TiO<sub>2</sub> anatase phase is significantly lower than that for the rutile phase [45]. Thus, it was observed that with the increase of Zn in the electrolyte, which gradually increased the energy of the MAO process, the amount of anatase phase decreased, while other phases, which require more energy for formation, increased. The research conducted by Zhang et al. modified the energy of the MAO treatment by changing the electrolyte composition [46] and varying the applied current density [41]. In both cases,

with increasing the energy involved in the process, the TiO<sub>2</sub> rutile phase increased, while the anatase phase decreased. Due to the high temperatures in the coating production process and very high cooling rate [47–49], the produced surface was characterized by low crystallinity, ranging between 10.6 and 18.4%. Other studies have also shown the low crystallinity of MAO coatings [50–52]. Komarova et al. [4] demonstrated that adding Zn caused a slight increase in the crystallinity of the coating produced on the Ti-40Nb alloy, although the coating was mainly amorphous. Kuroda et al. [13] studied the effect of thermal treatments on MAO coatings and observed that, even at high temperatures (800 °C), the coating remained amorphous.

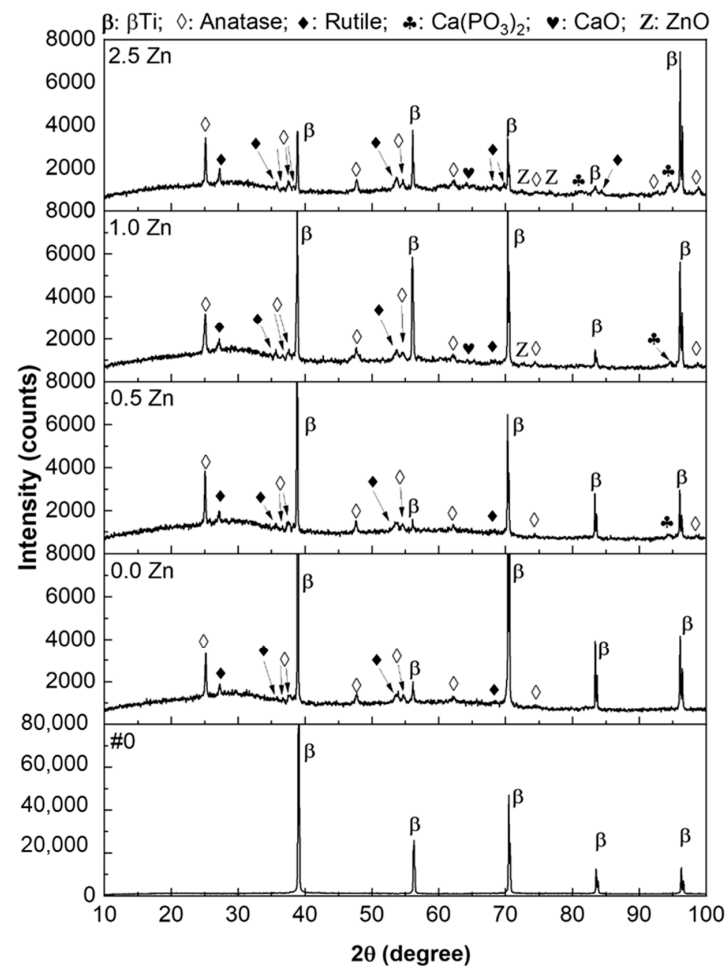


**Figure 5.** XRD patterns of the Ti-30Nb-5Mo alloy substrate and the MAO coatings.

Figure 7 shows the high-resolution XPS spectra of the alloying elements incorporated during the MAO process to determine the oxidation state of the elements.

Upon the Ti peaks deconvolution, the doublet relative to TiO<sub>2</sub> was observed, with a peak (2p<sub>3/2</sub>) at 458.5 eV [53]. The Nb spectrum showed the Nb<sub>2</sub>O<sub>5</sub> peaks of the 3d, 3d<sub>5/2</sub>, and 3d<sub>3/2</sub> doublets at 207.1 eV [47]. From the Ca spectrum, the peaks related to the CaCO<sub>3</sub> doublet were observed at 347.2 eV [54]. For P, the spectrum showed incorporation of ions in the phosphate form (PO<sub>4</sub>)<sup>3−</sup> at 133 eV [55]. In the Mg spectrum, the MgCO<sub>3</sub> peak was observed at 1305 eV [51]. The O1s spectrum showed the peaks of the metallic oxides (Ti and Nb) at 531.5 eV and from hydroxide (OH) at 533.6 eV. Due to the use of acetates in the electrolyte, contamination by carbon occurs. Therefore, the C1s spectrum showed peaks of C-C, C-O-C, and O-C=O bonds at 284.8 eV, 286.4 eV, and 288.6 eV, respectively [56]. Finally, the Zn 2p<sub>3/2</sub> spectrum presented peaks at 1022 eV, indicating the presence of Zn<sup>2+</sup> [57]. No peak associated with the Mo alloying element was detected due to its low concentration in the substrate (5 wt%), and due to the fact that it is a non-valve metal. This makes its

oxidation by MAO less favorable kinetically, as the driving force for its oxidation is similar to or lower than that of hydrogen being converted to water [58].

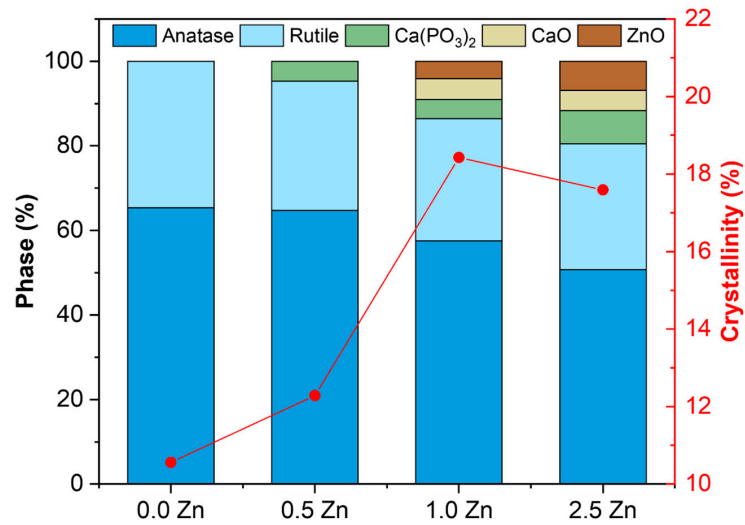


Figure 6. Phase composition and crystallinity of the MAO coatings.

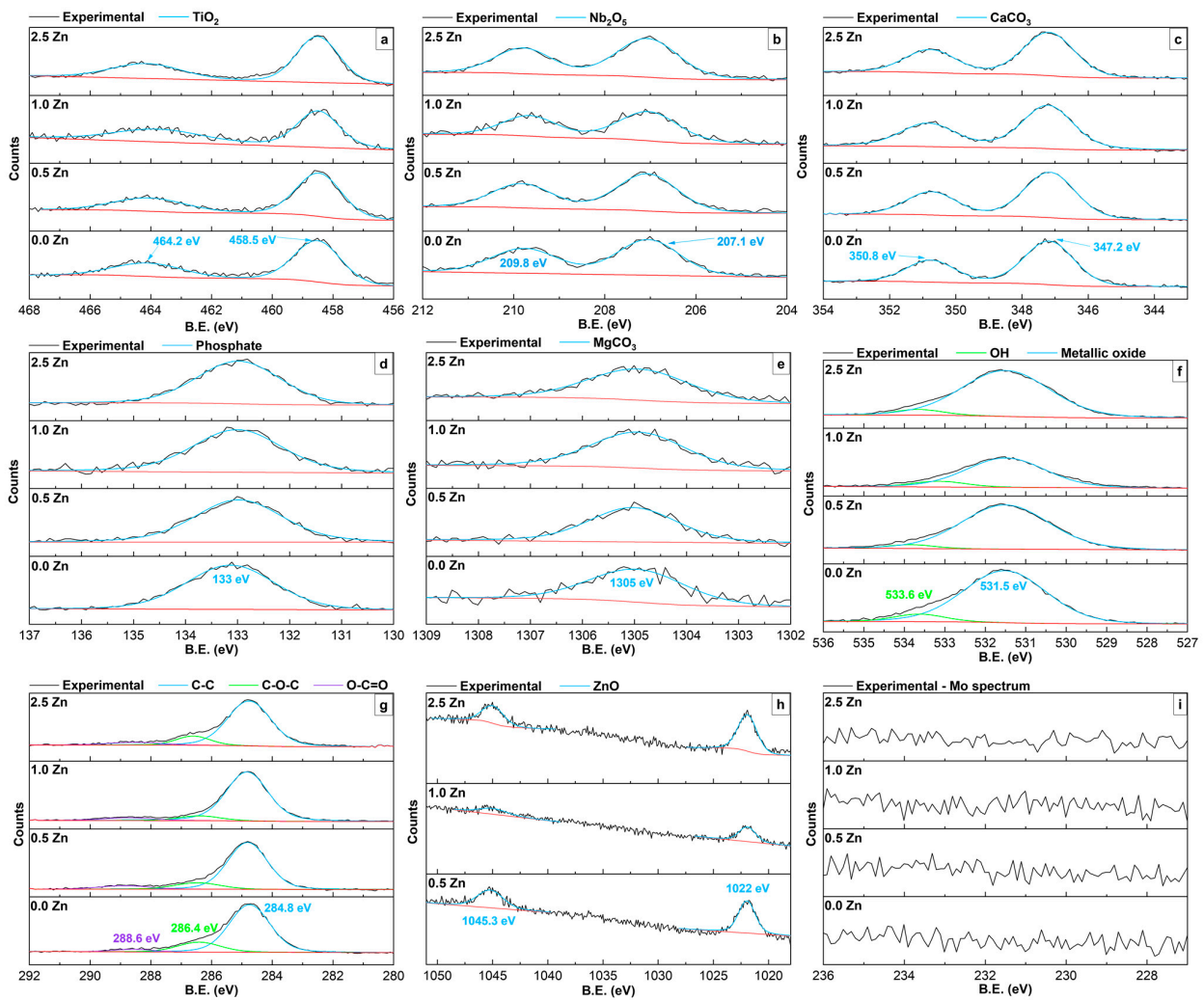


Figure 7. High-resolution XPS of the alloying elements (Ti (a), Nb (b), and Mo (i)) and Ca (c), P (d), Mg (e), O (f), C (g), and Zn (h) in the outer layer of the samples. The red lines are the background lines.

The same peaks identified in this study were also identified by Kuroda et al., ( $\text{TiO}_2$ , and  $\text{Nb}_2\text{O}_5$ ) [47], Costa et al., ( $\text{TiO}_2$ ,  $\text{CaCO}_3$ ,  $\text{PO}_4^{3-}$ , and  $\text{OH}$ ) [59], Sousa et al., ( $\text{TiO}_2$ ,  $\text{CaCO}_3$ ,  $\text{PO}_4^{3-}$ , and  $\text{MgCO}_3$ ) [51], and Leśniak-Ziółkowska et al., ( $\text{TiO}_2$ ,  $\text{PO}_4^{3-}$ ,  $\text{Zn}^{2+}$ , and carbon bonds) [57].

Table 2 presents the atomic percentage of the elements detected by the XPS analysis. It is observed that the relatively low concentration of Zn is due to the non-uniform distribution of this element in the coating. In the MAO process, the elements present in the electrolyte are transported through a short circuit, leading to their incorporation into the resulting oxide. In this way, the elements tend to be incorporated into the coating through defects, such as discharge channels, pores, and cracks. The accumulation of particles on the surface of the coating, observed in the SEM images, suggested that the energy level during the process was not relatively high to allow the diffusion of the elements. As a result, there were fewer defects, and it was more difficult to incorporate Zn uniformly [41].

**Table 2.** Quantification of elements obtained by XPS.

Element	0.0 Zn	0.5 Zn	1.0 Zn	2.5 Zn
Ca (at %)	$(7.10 \pm 0.22)$	$(8.73 \pm 0.35)$	$(5.85 \pm 0.14)$	$(6.19 \pm 0.52)$
P (at %)	$(10.7 \pm 2.8)$	$(8.8 \pm 2.4)$	$(4.8 \pm 1.1)$	$(10.1 \pm 3.2)$
Mg (at %)	$(0.60 \pm 0.88)$	$(2.5 \pm 2.9)$	$(2.2 \pm 2.6)$	$(3.3 \pm 3.6)$
C (at %)	$(44.2 \pm 5.9)$	$(42.8 \pm 4.5)$	$(62.6 \pm 5.7)$	$(35.1 \pm 4.8)$
O (at %)	$(34.7 \pm 9.1)$	$(33.7 \pm 8.3)$	$(23.8 \pm 7.2)$	$(40.8 \pm 9.0)$
Ti (at %)	$(1.93 \pm 0.87)$	$(2.41 \pm 0.66)$	$(0.54 \pm 0.20)$	$(3.35 \pm 0.60)$
Nb (at %)	$(0.84 \pm 0.25)$	$(0.94 \pm 0.31)$	$(0.23 \pm 0.01)$	$(0.94 \pm 0.35)$
Zn (at %)	-	$(0.14 \pm 0.13)$	$(0.02 \pm 0.02)$	$(0.19 \pm 0.19)$

### 3.3. Surface Roughness

The AFM images and the surface roughness of the samples are shown in Figure 8. The average roughness tends to increase with the addition of Zn in the electrolyte. This is a consequence of the gradual increase in the energy of the MAO process, due to the increase in the number of ions in the electrolytic solution [43]. The same trend of increased roughness with increasing amounts of Zn was observed by Zhang et al. [10]. However, the values obtained in [10] are higher than those obtained in the present study with the Ti-30Nb-5Mo alloy. Another indication is that the energy of the MAO process for this alloy is relatively smaller, corroborating the SEM results (accumulation of particles on the surface) and the chemical composition determined by XPS (low Zn concentration).

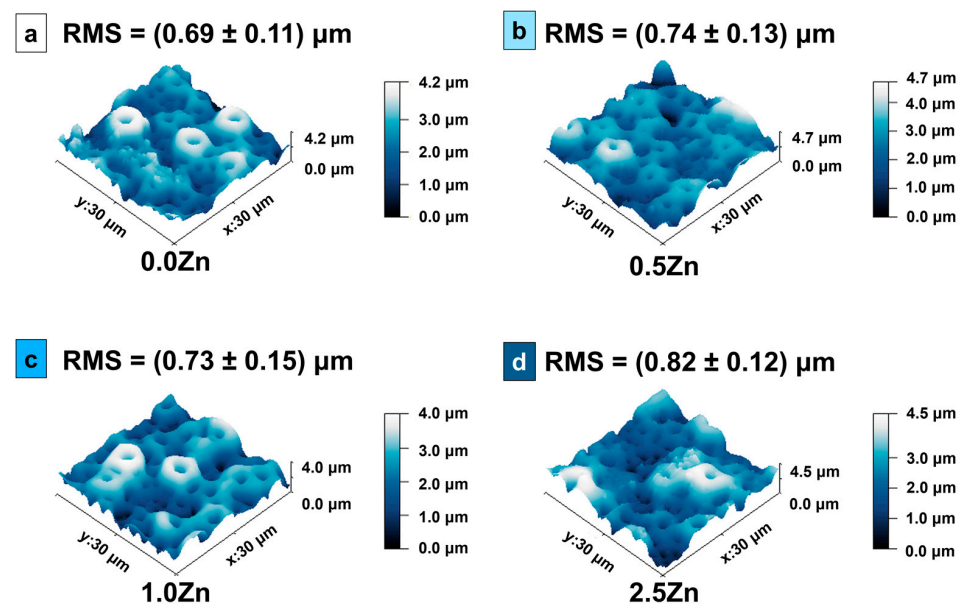


**Figure 8.** 3D topography images and surface roughness of 0.0 Zn (a), 0.5 Zn (b), 1.0 Zn (c), and 2.5 Zn (d) samples.

### 3.4. Wettability

The surface samples' contact angles are shown in Figure 9. All surfaces are hydrophilic ( $<90^\circ$ ). Compared to the surface without the MAO treatment (#0), the porous surface slightly decreased the water drop contact angle in the sample without Zn (0.0 Zn). For the 0.5 Zn sample, the amount of Zn added to the electrolyte solution was not enough to change the value of its contact angle. However, as the Zn concentration increased, the contact angle progressively decreased.  $\text{TiO}_2$  (anatase and rutile) is a hydrophilic substance [60]. Thus, as the oxidation of the Ti alloy by the MAO produces this oxide on the surface, the contact angle of the treated samples tends to decrease in comparison with the substrate. Roughness, on the other hand, is another factor that alters the wettability of the samples, and a rougher surface has a greater contact area, increasing the free energy, which makes it more hydrophilic [61,62]. Also, the pores absorb the water deposited on the surface due to the three-dimensional capillary effect [61]. Zhang et al. observed that an increase in Zn amount in the electrolyte used in the MAO treatment caused an increase in roughness and a decrease in the surface contact angle of the Ti-6Al-4V alloy [10]. Xu et al. [63] varied the oxidation time of CP-Ti samples and observed a decreasing trend in the contact angle as the increase in treatment time made the surface more rough.

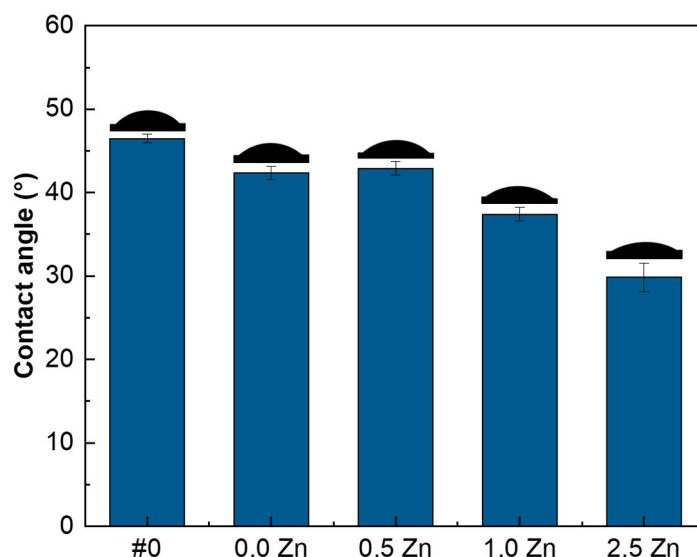


**Figure 9.** Contact angle of the Ti-30Nb-5Mo alloy substrate (#0) and the MAO coatings.

### 3.5. Antimicrobial Activity

The results of the growth of different microorganisms (*E. coli*, *S. aureus*, *E. faecalis*, *P. aeruginosa*, and *C. albicans*) on the samples' surfaces are shown in Figures 10–14, respectively. The most common microorganisms involved in surgical infections were chosen for this study. A similar choice was made also in other literature references [64–67].

Concerning the *E. coli* bacteria control, only the substrate (#0) had significantly lower bacterial growth. With the MAO treatment and, subsequently, with the addition of Zn, the growth of *E. coli* increased as the Zn concentration increased, reaching values very close to the control.

Only the 0.5 Zn sample had a significantly lower growth of *S. aureus* bacteria strain than the control, although it is possible to observe an apparent downward trend in this bacteria growth rate as the Zn concentration increased. However, the variation in Zn levels was insufficient to observe a greater interference with the results for the *S. aureus*.

The growth of the *E. faecalis* in the samples was highly impaired by the performed MAO treatments, since all the samples that went through this process had significantly lower bacterial growth than the control. By increasing the Zn concentration, the growth of the *E. faecalis* bacteria gradually decreased. The growth of *E. faecalis* in the 2.5 Zn sample was significantly lower than in the 0.0 Zn and 0.5 Zn samples.

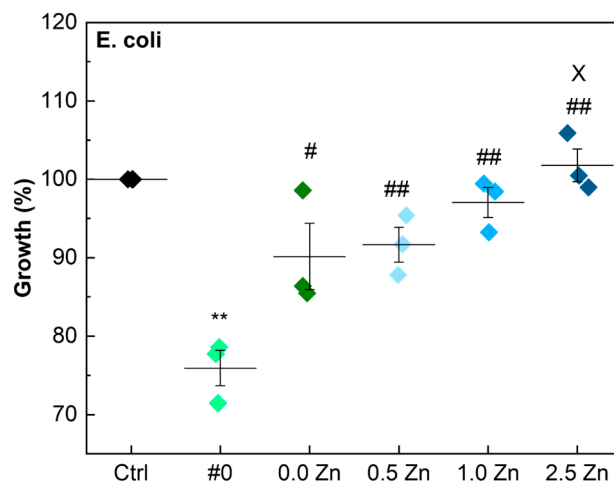


**Figure 10.** *E. coli* growth on the Ti-30Nb-5Mo alloy substrate and on the MAO coatings (\*\*  $p < 0.01$ , compared with Ctrl group; #  $p < 0.05$ , ##  $p < 0.01$ , compared with #0 group; X  $p < 0.05$  compared with 0.5 Zn group).

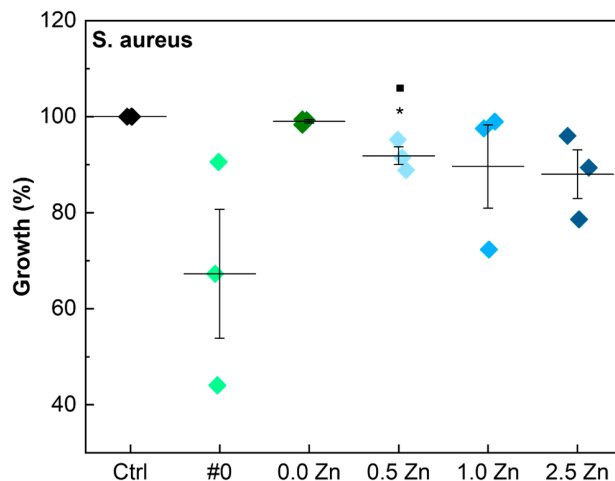


**Figure 11.** *S. aureus* growth on the Ti-30Nb-5Mo alloy substrate and on the MAO coatings (\*  $p < 0.05$ , compared with Ctrl group; ■  $p < 0.05$ , compared with 0.0 Zn group).

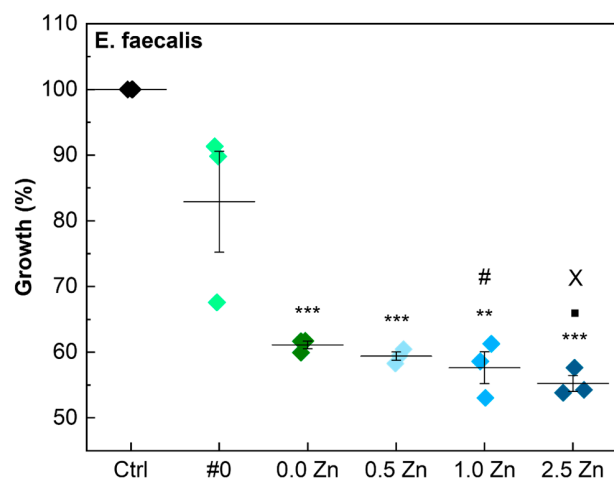


**Figure 12.** *E. faecalis* growth on the Ti-30Nb-5Mo alloy substrate and on the MAO coatings (\*\*  $p < 0.01$ , \*\*\*  $p < 0.001$ , compared with Ctrl group; #  $p < 0.05$ , compared with #0 group; ■  $p < 0.05$ , compared with 0.0 Zn group; X  $p < 0.05$ , compared with 0.5 Zn group).

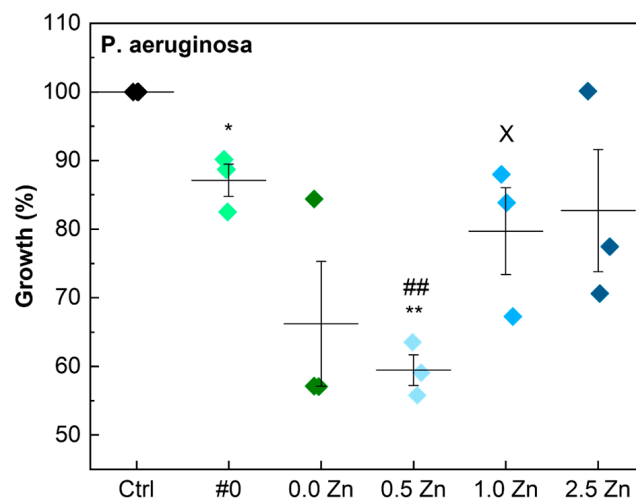


**Figure 13.** *P. aeruginosa* growth on the Ti-30Nb-5Mo alloy substrate and on the MAO coatings (\*  $p < 0.05$ , \*\*  $p < 0.01$ , compared with Ctrl group; ##  $p < 0.01$ , compared with #0 group; X  $p > 0.05$ , compared with 0.5 Zn group).

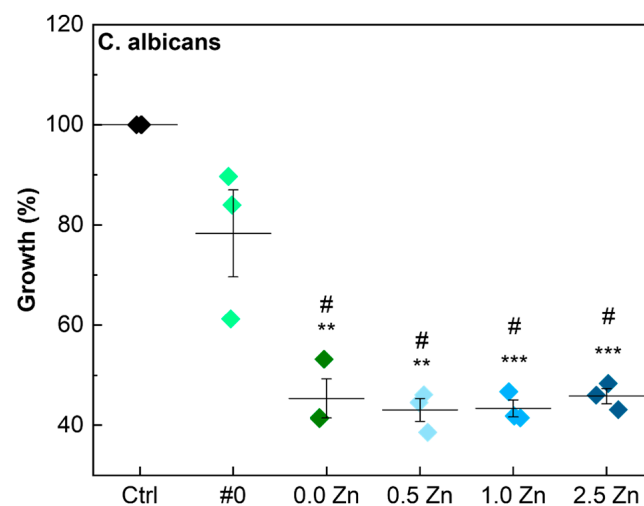


**Figure 14.** *C. albicans* growth on the Ti-30Nb-5Mo alloy substrate and on the MAO coatings (\*\*  $p < 0.01$ , \*\*\*  $p < 0.001$ , compared with Ctrl group; #  $p < 0.05$ , compared with #0 group).

The MAO treatment without Zn particles successfully prevented the growth of *P. aeruginosa* bacteria. However, as the amount of the added Zn increased, the effectiveness of the treatment decreased, reaching values that were similar to the control.

Finally, all the performed MAO treatments were effective against the growth of the *C. albicans* fungus, and the variation in Zn levels in the used electrolyte solution had no apparent influence on the results.

The substrate sample (#0), which did not undergo the MAO oxidation process, could reduce the growth of all the microorganisms tested. This result may be related to the bactericidal effect of molybdenum. Kawakami et al. studied the bactericidal effect of several commercially pure metals. They concluded that Mo has a bactericidal effect against *E. coli* and *S. aureus*. The antimicrobial activity of Mo (5.45) is close to that of silver (5.44) for the *E. coli* bacteria strain [68]. However, the authors did not investigate the impact of the metals on other types of bacteria [68].

Although Zn is known to possess antibacterial properties, other factors can influence the adhesion of microorganisms to the sample surface. The wettability, chemical composition, porosity, and roughness of the samples can influence the adhesion of bacteria to the surface. In particular, the probability of adhesion of microorganisms is higher on

rough rather than on smooth surfaces [66,67]. Although favorable for cell adhesion, the hydrophilicity of the samples also contributes to the adhesion of bacteria, and the amount of Zn added to the samples may not be sufficient to eliminate this effect [65]. Leśniak-Ziółkowska et al. [57] investigated the antibacterial properties of oxides containing Zn produced via MAO on the Ti-15Mo alloy and found that the amount of *S. aureus* increased after the surface treatment. This outcome could be due to the surfaces' roughness or solid particles in the coatings, which can also create a suitable environment for bacterial adhesion. These characteristics were verified in the Ti-30Nb-5Mo alloy samples treated by the MAO in the present study.

### 3.6. AMSC Viability

The results of the MTT tests performed on samples treated with the MAO, with and without Zn particles in the electrolyte solution are shown in Figure 15. The data obtained for samples #0, 0.0 Zn and 0.5 Zn are close to the control, showing no great interference with the AMSC growth. However, the addition of higher amounts of Zn (1.0 Zn and 2.5 Zn) led to an increase in the AMSC growth on the surface of the samples. In addition, the results demonstrated that the addition of Zn did not have any cytotoxic effect during in vitro testing. The rough and porous surface produced by the MAO treatment facilitates the adhesion and proliferation of osteoblastic cells [69–71]. Hydrophilic surfaces also influence cell adhesion and proliferation on the surface of the samples, consequently improving the bone healing process [62]. This was studied and verified by Park et al. [72] and Rupp et al. [73]. Regarding improving cell adhesion results of 1.0 Zn and 2.5 Zn samples, some studies report that the addition of Zn can positively influence cell proliferation and viability [57,74,75].

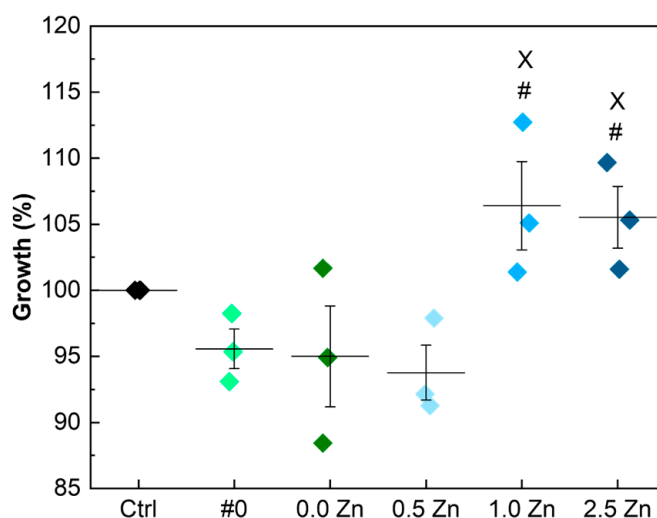


**Figure 15.** AMSC growth on the substrate and on the MAO coatings (#  $p < 0.05$ , compared with #0 group; X  $p < 0.05$ , compared with 0.5 Zn group).

### 3.7. Osteogenic Differentiation

The images of the cell monolayers in the different samples after staining with Alizarin Red S, which highlights in red the calcium deposits, are presented in Figure 16. The positive control is represented by the AMSCs (without substrate) differentiated into the osteogenic lineage, while the undifferentiated AMSCs represent the negative control. All the images are comparable with the positive control (+Ctrl). Therefore, all the investigated samples do not disturb the differentiation into the AMSC osteogenic lineage.

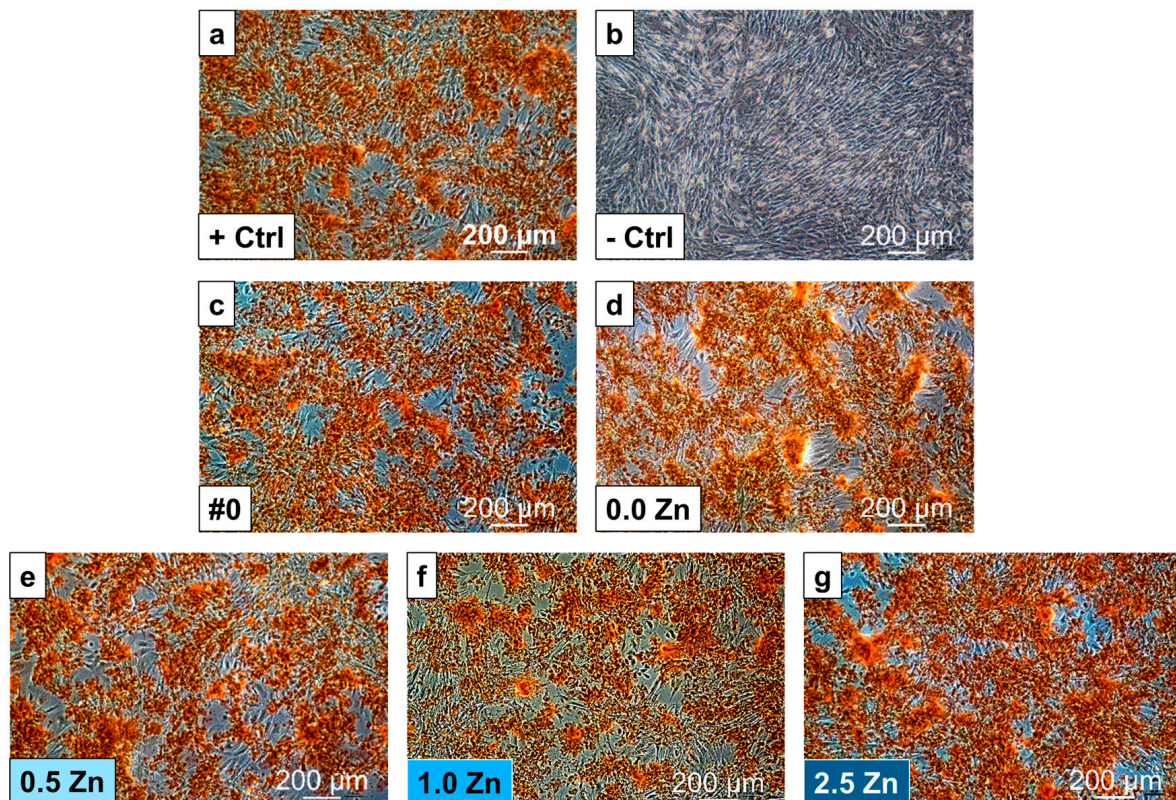


**Figure 16.** Alizarin Red S staining of AMSCs differentiated in vitro into the osteogenic lineage for positive control (a), negative control (b), substrate (c), and 0.0 Zn (d), 0.5 Zn (e), 1.0 Zn (f), and 2.5 Zn (g) MAO coatings.

#### 4. Conclusions

From the results obtained in this study, it can be concluded that it is possible to incorporate Zn into the surface of the Ti-30Nb-5Mo alloy through the MAO technique. The relatively low energy of the MAO process and the short treatment time led to the inhomogeneous Zn incorporation. With the increase of the Zn concentration in the electrolyte, the treatment energy increased due to the increase in the total amount of ions in the electrolyte solution. The incorporation of Ca, P, Mg, and Zn into the coating increased with the increase of Zn content in the electrolyte. With the increase of Zn, the coatings' porosity, roughness, and crystallinity increased from 14.2 to 17.1%, 0.69 to 0.82  $\mu\text{m}$ , and 10.6 to 17.6%, respectively. The Zn incorporation reduced the *E. faecalis*, *P. aeruginosa*, and *C. albicans* growth on the samples' surfaces, with 2.5 Zn sample presenting (55.2  $\pm$  1.3)%, (82.7  $\pm$  8.9)%, and (45.8  $\pm$  1.6)% growth, respectively. The increase of the roughness and decrease of the contact angle (from 46.5 to 29.8°) with the Zn increase promoted higher *E. coli* and *S. aureus* adhesion, being necessary to increase the Zn incorporation to nullify the contributions of the surface characteristics to the growth of microorganisms. The addition of Zn to the surface of the Ti-30Nb-5Mo alloy promoted the AMSC growth by (105.5  $\pm$  2.4)% and (106.4  $\pm$  3.3)%, for 1.0 Zn and 2.5 Zn samples, respectively. The variation in the Zn concentration had no impact on the osteogenic differentiation of the AMSC, and all samples were comparable to the positive control (without substrate).

**Author Contributions:** Conceptualization, G.C.C.; methodology, G.C.C., K.B., P.A.B.K., L.I., A.D.B., R.T., M.C., E.I. and V.Y.G.; investigation, G.C.C., K.B., P.A.B.K., L.I., A.D.B., R.T., M.C. and E.I.; validation, G.V.; resources, C.R.G. and J.V.R.; writing—original draft preparation, G.C.C.; writing—review and editing, P.A.B.K., C.R.G. and J.V.R.; supervision, C.R.G. and J.V.R.; project administration, C.R.G. and J.V.R.; funding acquisition, C.R.G. and J.V.R. All authors have read and agreed to the published version of the manuscript.

**Funding:** This research was funded by Coordenação de Aperfeiçoamento de Pessoal de Nível Superior—Brazil (CAPES) (grant #88887.716787/2022-00) and Conselho Nacional de Desenvolvimento Científico e Tecnológico (CNPq) (Grant #314.810/2021-8).

**Institutional Review Board Statement:** Not applicable.

**Informed Consent Statement:** Not applicable.

**Data Availability Statement:** The obtained data are available upon a reasonable request to the corresponding author.

**Acknowledgments:** The authors would like to thank Fenelon Martinho Lima Pontes for the XRD measurements. The technical support of Massimo Di Menno Di Bucchianico and Marco Ortenzi is gratefully acknowledged.

**Conflicts of Interest:** The authors declare that they are not aware of competition for financial interest or personal relationships that may have influenced the work reported in this paper.

## References

1. Li, G.; Zhao, Q.-M.; Yang, H.-L.; Cheng, L. Antibacterial and Microstructure Properties of Titanium Surfaces Modified with Ag-Incorporated Nanotube Arrays. *Mater. Res.* **2016**, *19*, 735–740. [[CrossRef](#)]
2. Shimabukuro, M. Antibacterial Property and Biocompatibility of Silver, Copper, and Zinc in Titanium Dioxide Layers Incorporated by One-Step Micro-Arc Oxidation: A Review. *Antibiotics* **2020**, *9*, 716. [[CrossRef](#)]
3. Darouiche, R.O. Treatment of Infections Associated with Surgical Implants. *N. Engl. J. Med.* **2004**, *350*, 1422–1429. [[CrossRef](#)]
4. Komarova, E.G.; Sharkeev, Y.P.; Sedelnikova, M.B.; Prosolov, K.A.; Khlusov, I.A.; Prymak, O.; Epple, M. Zn- or Cu-Containing CaP-Based Coatings Formed by Micro-arc Oxidation on Titanium and Ti-40Nb Alloy: Part I—Microstructure, Composition and Properties. *Materials* **2020**, *13*, 4116. [[CrossRef](#)]
5. Nikoomanzari, E.; Karbasi, M.; Melo, W.C.M.A.; Moris, H.; Babaei, K.; Giannakis, S.; Fattah-alhosseini, A. Impressive strides in antibacterial performance amelioration of Ti-based implants via plasma electrolytic oxidation (PEO): A review of the recent advancements. *Chem. Eng. J.* **2022**, *441*, 136003. [[CrossRef](#)]
6. Fattah-alhosseini, A.; Molaei, M.; Attarzadeh, N.; Babaei, K.; Attarzadeh, F. On the enhanced antibacterial activity of plasma electrolytic oxidation (PEO) coatings that incorporate particles: A review. *Ceram. Int.* **2020**, *46*, 20587–20607. [[CrossRef](#)]
7. Rizwan, M.; Alias, R.; Zaidi, U.Z.; Mahmoodian, R.; Hamdi, M. Surface modification of valve metals using plasma electrolytic oxidation for antibacterial applications: A review. *J. Biomed. Mater. Res. Part A* **2018**, *106*, 590–605. [[CrossRef](#)] [[PubMed](#)]
8. Wolcott, R.D.; Ehrlich, G.D. Biofilms and Chronic Infections. *JAMA* **2008**, *299*, 2682–2684. [[CrossRef](#)] [[PubMed](#)]
9. Kirmanidou, Y.; Sidira, M.; Drosou, M.-E.; Bennani, V.; Bakopoulou, A.; Tsouknidas, A.; Michailidis, N.; Michalakis, K. New Ti-alloys and surface modifications to improve the mechanical properties and the biological response to orthopedic and dental implants: A review. *BioMed Res. Int.* **2016**, *2016*, 2908570. [[CrossRef](#)]
10. Zhang, Z.-Y.; Huang, T.-Y.; Zhai, D.-J.; Wang, H.-B.; Feng, K.-Q.; Xiang, L. Study on Zn-doped antibacterial bioactive coatings on Ti6Al4V titanium alloy surfaces by micro-arc oxidation. *Surf. Coat. Technol.* **2023**, *467*, 129724. [[CrossRef](#)]
11. Grigoriev, S.; Sotova, C.; Vereschaka, A.; Uglov, V.; Cherenda, N. Modifying Coatings for Medical Implants Made of Titanium Alloys. *Metals* **2023**, *13*, 718. [[CrossRef](#)]
12. Bloyce, A. Surface engineering of titanium alloys for wear protection. *Proc. Inst. Mech. Eng. Part J J. Eng. Tribol.* **1998**, *212*, 467–476. [[CrossRef](#)]
13. Kuroda, P.A.B.; de Mattos, F.N.; Grandini, C.R.; Afonso, C.R.M. Influence of the heat treatment temperature on the MAO coating produced in the Ti-25Ta-25Zr alloy. *J. Mater. Res. Technol.* **2023**, *26*, 3881–3892. [[CrossRef](#)]
14. Kuroda, P.A.B.; de Mattos, F.N.; Grandini, C.R.; Afonso, C.R.M. Micro-abrasive wear behavior by ball cratering on MAO coating of Ti-25Ta alloy. *J. Mater. Res. Technol.* **2023**, *26*, 1850–1855. [[CrossRef](#)]
15. Jiang, B.L.; Ge, Y.F. Micro-arc oxidation (MAO) to improve the corrosion resistance of magnesium (Mg) alloys. In *Corrosion Prevention of Magnesium Alloys*; Woodhead Publishing Series in Metals and Surface Engineering; Woodhead Publishing: Cambridge, UK, 2013; pp. 163–196. [[CrossRef](#)]
16. Liu, S.; Chen, J.; Zhang, D.; Wang, Y.; He, Z.; Guo, P. Properties of Micro-Arc Oxidation Coatings on 5052 Al Alloy Sealed by SiO<sub>2</sub> Nanoparticles. *Coatings* **2022**, *12*, 373. [[CrossRef](#)]
17. Chen, W.-W.; Wang, Z.-X.; Sun, L.; Lu, S. Research of growth mechanism of ceramic coatings fabricated by micro-arc oxidation on magnesium alloys at high current mode. *J. Magnes. Alloys* **2015**, *3*, 253–257. [[CrossRef](#)]
18. Liu, S.; Li, B.; Liang, C.; Wang, H.; Qiao, Z. Formation mechanism and adhesive strength of a hydroxyapatite/TiO<sub>2</sub> composite coating on a titanium surface prepared by micro-arc oxidation. *Appl. Surf. Sci.* **2016**, *362*, 109–114. [[CrossRef](#)]
19. Ping, W.; Ting, W.; Hao, P.; Yang, G.X. Effect of NaAlO<sub>2</sub> concentrations on the properties of micro-arc oxidation coatings on pure titanium. *Mater. Lett.* **2016**, *170*, 171–174. [[CrossRef](#)]
20. Naji Chabuk, Q.K.; Salman Al-Murshdy, J.M.; Dawood, N.M. Review: The Surface Modification of Pure Titanium by Micro-Arc Oxidation (MAO) Process. *J. Phys. Conf. Ser.* **2021**, *1973*, 012114. [[CrossRef](#)]

21. Rossi, M.C.; dos Santos, R.F.; Kuroda, P.A.B.; Afonso, C.R.M. Characteristics of ceramic-like coatings obtained by plasma electrolyte oxidation on different Ti alloys. *Boletín Soc. Española Cerámica Vidr.* **2023**. [[CrossRef](#)]
22. Park, M.-G.; Choe, H.-C. Corrosion behaviors of bioactive element coatings on PEO-treated Ti-6Al-4V alloys. *Surf. Coat. Technol.* **2019**, *376*, 44–51. [[CrossRef](#)]
23. Zhang, X.; Li, M.; He, X.; Huang, X.; Hang, R.; Tang, B. Effects of silver concentrations on microstructure and properties of nanostructured titania films. *Mater. Des.* **2015**, *65*, 600–605. [[CrossRef](#)]
24. Zhang, X.; Li, M.; He, X.; Hang, R.; Huang, X.; Wang, Y.; Yao, X.; Tang, B. Antibacterial activity of single crystalline silver-doped anatase TiO<sub>2</sub> nanowire arrays. *Appl. Surf. Sci.* **2016**, *372*, 139–144. [[CrossRef](#)]
25. Huang, Q.; Li, X.; Elkhooly, T.A.; Liu, X.; Zhang, R.; Wu, H.; Feng, Q.; Liu, Y. The Cu-containing TiO<sub>2</sub> coatings with modulatory effects on macrophage polarization and bactericidal capacity prepared by micro-arc oxidation on titanium substrates. *Colloids Surf. B Biointerfaces* **2018**, *170*, 242–250. [[CrossRef](#)] [[PubMed](#)]
26. Huang, Q.; Ouyang, Z.; Tan, Y.; Wu, H.; Liu, Y. Activating macrophages for enhanced osteogenic and bactericidal performance by Cu ion release from micro/nano-topographical coating on a titanium substrate. *Acta Biomater.* **2019**, *100*, 415–426. [[CrossRef](#)]
27. Fosca, M.; Streza, A.; Antoniac, I.V.; Vadalà, G.; Rau, J.V. Ion-Doped Calcium Phosphate-Based Coatings with Antibacterial Properties. *J. Funct. Biomater.* **2023**, *14*, 250. [[CrossRef](#)]
28. Zhang, X.; Wang, H.; Li, J.; He, X.; Hang, R.; Huang, X.; Tian, L.; Tang, B. Corrosion behavior of Zn-incorporated antibacterial TiO<sub>2</sub> porous coating on titanium. *Ceram. Int.* **2016**, *42*, 17095–17100. [[CrossRef](#)]
29. Zhang, W.; Zhang, S.; Liu, H.; Ren, L.; Wang, Q.; Zhang, Y. Effects of surface roughening on antibacterial and osteogenic properties of Ti-Cu alloys with different Cu contents. *J. Mater. Sci. Technol.* **2021**, *88*, 158–167. [[CrossRef](#)]
30. Fadeeva, I.V.; Deyneko, D.V.; Knotko, A.V.; Olkhov, A.A.; Slukin, P.V.; Davydova, G.A.; Trubitsyna, T.A.; Preobrazhenskiy, I.I.; Gosteva, A.N.; Antoniac, I.V.; et al. Antibacterial Composite Material Based on Polyhydroxybutyrate and Zn-Doped Brushite Cement. *Polymers* **2023**, *15*, 2106. [[CrossRef](#)]
31. Fadeeva, I.V.; Goldberg, M.A.; Preobrazhenskiy, I.I.; Mamin, G.V.; Davidova, G.A.; Agafonova, N.V.; Fosca, M.; Russo, F.; Barinov, S.M.; Cavalu, S.; et al. Improved cytocompatibility and antibacterial properties of zinc-substituted brushite bone cement based on  $\beta$ -tricalcium phosphate. *J. Mater. Sci. Mater. Med.* **2021**, *32*, 99. [[CrossRef](#)]
32. Ye, J.; Li, B.; Li, M.; Zheng, Y.; Wu, S.; Han, Y. ROS induced bactericidal activity of amorphous Zn-doped titanium oxide coatings and enhanced osseointegration in bacteria-infected rat tibias. *Acta Biomater.* **2020**, *107*, 313–324. [[CrossRef](#)]
33. Zhu, D.; Su, Y.; Young, M.L.; Ma, J.; Zheng, Y.; Tang, L. Biological Responses and Mechanisms of Human Bone Marrow Mesenchymal Stem Cells to Zn and Mg Biomaterials. *ACS Appl. Mater. Interfaces* **2017**, *9*, 27453–27461. [[CrossRef](#)]
34. Lowe, N.M.; Fraser, W.D.; Jackson, M.J. Is there a potential therapeutic value of copper and zinc for osteoporosis? *Proc. Nutr. Soc.* **2009**, *61*, 181–185. [[CrossRef](#)] [[PubMed](#)]
35. Cardoso, G.C.; de Almeida, G.S.; Corrêa, D.O.G.; Zambuzzi, W.F.; Buzalaf, M.A.R.; Correa, D.R.N.; Grandini, C.R. Preparation and characterization of novel as-cast Ti-Mo-Nb alloys for biomedical applications. *Sci. Rep.* **2022**, *12*, 11874. [[CrossRef](#)]
36. Cardoso, G.C.; Buzalaf, M.A.R.; Correa, D.R.N.; Grandini, C.R. Effect of Thermomechanical Treatments on Microstructure, Phase Composition, Vickers Microhardness, and Young's Modulus of Ti-xNb-5Mo Alloys for Biomedical Applications. *Metals* **2022**, *12*, 788.
37. Cardoso, G.C.; Kuroda, P.A.B.; Grandini, C.R. Influence of Nb addition on the structure, microstructure, Vickers microhardness, and Young's modulus of new  $\beta$  Ti-xNb-5Mo alloys system. *J. Mater. Res. Technol.* **2023**, *25*, 3061–3070. [[CrossRef](#)]
38. Rabadia, C.D.; Liu, Y.J.; Cao, G.H.; Li, Y.H.; Zhang, C.W.; Sercombe, T.B.; Sun, H.; Zhang, L.C. High-strength  $\beta$  stabilized Ti-Nb-Fe-Cr alloys with large plasticity. *Mater. Sci. Eng. A* **2018**, *732*, 368–377. [[CrossRef](#)]
39. Wang, Y.B.; Zheng, Y.F. Corrosion behaviour and biocompatibility evaluation of low modulus Ti-16Nb shape memory alloy as potential biomaterial. *Mater. Lett.* **2009**, *63*, 1293–1295. [[CrossRef](#)]
40. Roknian, M.; Fattah-alhosseini, A.; Gashti, S.O.; Keshavarz, M.K. Study of the effect of ZnO nanoparticles addition to PEO coatings on pure titanium substrate: Microstructural analysis, antibacterial effect and corrosion behavior of coatings in Ringer's physiological solution. *J. Alloys Compd.* **2018**, *740*, 330–345. [[CrossRef](#)]
41. Zhang, X.; Yang, L.; Lu, X.; Lv, Y.; Jiang, D.; Yu, Y.; Peng, Z.; Dong, Z. Characterization and property of dual-functional Zn-incorporated TiO<sub>2</sub> micro-arc oxidation coatings: The influence of current density. *J. Alloys Compd.* **2019**, *810*, 151893. [[CrossRef](#)]
42. Zhang, X.; Yu, Y.; Jiang, D.; Jiao, Y.; Wu, Y.; Peng, Z.; Zhou, J.; Wu, J.; Dong, Z. Synthesis and characterization of a bi-functional hydroxyapatite/Cu-doped TiO<sub>2</sub> composite coating. *Ceram. Int.* **2019**, *45*, 6693–6701. [[CrossRef](#)]
43. Li, G.; Ma, F.; Liu, P.; Qi, S.; Li, W.; Zhang, K.; Chen, X. Review of micro-arc oxidation of titanium alloys: Mechanism, properties and applications. *J. Alloys Compd.* **2023**, *948*, 169773. [[CrossRef](#)]
44. Lourenço, M.L.; Cardoso, G.C.; Sousa, K.d.S.J.; Donato, T.A.G.; Pontes, F.M.L.; Grandini, C.R. Development of novel Ti-Mo-Mn alloys for biomedical applications. *Sci. Rep.* **2020**, *10*, 6298. [[CrossRef](#)] [[PubMed](#)]
45. Chen, H.-T.; Hsiao, C.-H.; Long, H.-Y.; Chung, C.-J.; Tang, C.-H.; Chen, K.-C.; He, J.-L. Micro-arc oxidation of  $\beta$ -titanium alloy: Structural characterization and osteoblast compatibility. *Surf. Coat. Technol.* **2009**, *204*, 1126–1131. [[CrossRef](#)]
46. Zhang, X.; Li, C.; Yu, Y.; Lu, X.; Lv, Y.; Jiang, D.; Peng, Z.; Zhou, J.; Zhang, X.; Sun, S.; et al. Characterization and property of bifunctional Zn-incorporated TiO<sub>2</sub> micro-arc oxidation coatings: The influence of different Zn sources. *Ceram. Int.* **2019**, *45*, 19747–19756. [[CrossRef](#)]

47. Kuroda, P.A.B.; Grandini, C.R.; Afonso, C.R.M. Surface Characterization of New  $\beta$  Ti-25Ta-Zr-Nb Alloys Modified by Micro-Arc Oxidation. *Materials* **2023**, *16*, 2352. [[CrossRef](#)] [[PubMed](#)]
48. Sikora, M.S.; Carstensen, J.; Foll, H.; Pereira, E.C. Theoretical Calculation of the Local Heating Effect on the Crystallization of TiO<sub>2</sub> Prepared by Sparking Anodization. *Curr. Nanosci.* **2015**, *11*, 263–270. [[CrossRef](#)]
49. Chen, K.-T.; Huang, J.-W.; Lin, W.-T.; Kuo, T.-Y.; Chien, C.-S.; Chang, C.-P.; Lin, Y.-D. Effects of Micro-Arc Oxidation Discharge Parameters on Formation and Biomedical Properties of Hydroxyapatite-Containing Flower-like Structure Coatings. *Materials* **2023**, *16*, 57. [[CrossRef](#)]
50. Zhang, G.; Huang, S.; Li, X.; Zhao, D.; Cao, Y.; Liu, B.; Huang, Q. Oxide ceramic coatings with amorphous/nano-crystalline dual-structures prepared by micro-arc oxidation on Ti-Nb-Zr medium entropy alloy surfaces for biomedical applications. *Ceram. Int.* **2023**, *49*, 18114–18124. [[CrossRef](#)]
51. Sousa, T.S.P.; Costa, N.d.A.d.; Correa, D.R.N.; Rocha, L.A.; Grandini, C.R. Morphology, Crystalline Structure and Chemical Composition Of MAO Treated Ti-15Zr-Mo Surfaces Enriched with Bioactive Ions. *Mater. Res.* **2019**, *22*, 6. [[CrossRef](#)]
52. Kuroda, P.A.B.; Rossi, M.C.; Grandini, C.R.; Afonso, C.R.M. Assessment of applied voltage on the structure, pore size, hardness, elastic modulus, and adhesion of anodic coatings in Ca-, P-, and Mg-rich produced by MAO in Ti-25Ta-Zr alloys. *J. Mater. Res. Technol.* **2023**, *26*, 4656–4669. [[CrossRef](#)]
53. Kumari, P.; Saha, R.; Saikia, G.; Bhujel, A.; Choudhury, M.G.; Jagdale, P.; Paul, S. Synthesis of Mixed-Phase TiO<sub>2</sub>-ZrO<sub>2</sub> Nanocomposite for Photocatalytic Wastewater Treatment. *Toxics* **2023**, *11*, 234. [[CrossRef](#)] [[PubMed](#)]
54. Bilton, M.; Brown, A.P.; Milne, S.J. Investigating the optimum conditions for the formation of calcium oxide, used for CO<sub>2</sub> sequestration, by thermal decomposition of calcium acetate. *J. Phys. Conf. Ser.* **2012**, *371*, 012075. [[CrossRef](#)]
55. Hao, Y.; Ye, Z.; Wang, L.; Ye, M.; Dong, H.; Du, Y.; Wang, C. Dual-electrolyte fabrication of micro arc oxidation coatings on Ta-12W alloy with enhanced wear resistance. *Vacuum* **2023**, *211*, 111698. [[CrossRef](#)]
56. Skorupska, M.; Kamedulski, P.; Lukaszewicz, J.P.; Ilnicka, A. The Improvement of Energy Storage Performance by Sucrose-Derived Carbon Foams via Incorporating Nitrogen Atoms. *Nanomaterials* **2021**, *11*, 760. [[CrossRef](#)]
57. Leśniak-Ziółkowska, K.; Kazek-Kęsik, A.; Rokosz, K.; Raaen, S.; Stolarczyk, A.; Krok-Borkowicz, M.; Pamuła, E.; Gołda-Cepa, M.; Brzychczy-Włoch, M.; Simka, W. Electrochemical modification of the Ti-15Mo alloy surface in solutions containing ZnO and Zn<sub>3</sub>(PO<sub>4</sub>)<sub>2</sub> particles. *Mater. Sci. Eng. C* **2020**, *115*, 111098. [[CrossRef](#)] [[PubMed](#)]
58. Nie, X.; Cai, R.; Zhao, C.; Sun, J.; Zhang, J.; Matthews, D.T.A. Advancement of plasma electrolytic oxidation towards non-valve metals. *Surf. Coat. Technol.* **2022**, *442*, 128403. [[CrossRef](#)]
59. Costa, N.A.; Correa, D.R.N.; Lisboa-Filho, P.N.; Sousa, T.S.P.; Grandini, C.R.; Rocha, L.A. Influence of the molybdenum on characteristics of oxide films produced by micro-arc oxidation on Ti-15Zr-based alloys. *Surf. Coat. Technol.* **2021**, *408*, 126856. [[CrossRef](#)]
60. Zhang, L.; Zhao, N.; Xu, J. Fabrication and application of superhydrophilic surfaces: A review. *J. Adhes. Sci. Technol.* **2014**, *28*, 769–790. [[CrossRef](#)]
61. Zhang, Z.-Y.; Huang, T.-Y.; Zhai, D.-J.; Wang, H.-B.; Feng, K.-Q.; Xiang, L. Study on strontium doped bioactive coatings on titanium alloys surfaces by micro-arc oxidation. *Surf. Coat. Technol.* **2022**, *451*, 129045. [[CrossRef](#)]
62. Komarova, E.G.; Sharkeev, Y.P.; Sedelnikova, M.B.; Prymak, O.; Epple, M.; Litvinova, L.S.; Shupletsova, V.V.; Malashchenko, V.V.; Yurova, K.A.; Dzyuman, A.N.; et al. Zn- or Cu-containing CaP-Based Coatings Formed by Micro-Arc Oxidation on Titanium and Ti-40Nb Alloy: Part II—Wettability and Biological Performance. *Materials* **2020**, *13*, 4366. [[CrossRef](#)] [[PubMed](#)]
63. Xu, L.; Wu, C.; Lei, X.; Zhang, K.; Liu, C.; Ding, J.; Shi, X. Effect of oxidation time on cytocompatibility of ultrafine-grained pure Ti in micro-arc oxidation treatment. *Surf. Coat. Technol.* **2018**, *342*, 12–22. [[CrossRef](#)]
64. Geng, Z.; Wang, R.; Zhuo, X.; Li, Z.; Huang, Y.; Ma, L.; Cui, Z.; Zhu, S.; Liang, Y.; Liu, Y.; et al. Incorporation of silver and strontium in hydroxyapatite coating on titanium surface for enhanced antibacterial and biological properties. *Mater. Sci. Eng. C* **2017**, *71*, 852–861. [[CrossRef](#)]
65. Durdu, S.; Aktug, S.L.; Aktas, S.; Yalcin, E.; Cavusoglu, K.; Altinkok, A.; Usta, M. Characterization and in vitro properties of anti-bacterial Ag-based bioceramic coatings formed on zirconium by micro arc oxidation and thermal evaporation. *Surf. Coat. Technol.* **2017**, *331*, 107–115. [[CrossRef](#)]
66. Molaei, M.; Nouri, M.; Babaei, K.; Fattah-Alhosseini, A. Improving surface features of PEO coatings on titanium and titanium alloys with zirconia particles: A review. *Surf. Interfaces* **2021**, *22*, 100888. [[CrossRef](#)]
67. Nikoomanzari, E.; Fattah-alhosseini, A.; Pajohi Alamoti, M.R.; Keshavarz, M.K. Effect of ZrO<sub>2</sub> nanoparticles addition to PEO coatings on Ti-6Al-4V substrate: Microstructural analysis, corrosion behavior and antibacterial effect of coatings in Hank's physiological solution. *Ceram. Int.* **2020**, *46*, 13114–13124. [[CrossRef](#)]
68. Kawakami, H.; Yoshida, K.; Nishida, Y.; Kikuchi, Y.; Sato, Y. Antibacterial Properties of Metallic Elements for Alloying Evaluated with Application of JIS Z 2801:2000. *ISIJ Int.* **2008**, *48*, 1299–1304. [[CrossRef](#)]
69. Zhang, Y.-Y.; Zhu, Y.; Lu, D.-Z.; Dong, W.; Bi, W.-J.; Feng, X.-J.; Wen, L.-M.; Sun, H.; Qi, M.-C. Evaluation of osteogenic and antibacterial properties of strontium/silver-containing porous TiO<sub>2</sub> coatings prepared by micro-arc oxidation. *J. Biomed. Mater. Res. Part B Appl. Biomater.* **2021**, *109*, 505–516. [[CrossRef](#)]
70. Zhou, R.; Wei, D.; Cheng, S.; Feng, W.; Du, Q.; Yang, H.; Li, B.; Wang, Y.; Jia, D.; Zhou, Y. Structure, MC3T3-E1 Cell Response, and Osseointegration of Macroporous Titanium Implants Covered by a Bioactive Microarc Oxidation Coating with Microporous Structure. *ACS Appl. Mater. Interfaces* **2014**, *6*, 4797–4811. [[CrossRef](#)]

71. He, X.; Zhang, X.; Bai, L.; Hang, R.; Huang, X.; Qin, L.; Yao, X.; Tang, B. Antibacterial ability and osteogenic activity of porous Sr/Ag-containing TiO<sub>2</sub> coatings. *Biomed. Mater.* **2016**, *11*, 045008. [[CrossRef](#)]
72. Park, J.-W.; Jang, J.-H.; Lee, C.S.; Hanawa, T. Osteoconductivity of hydrophilic microstructured titanium implants with phosphate ion chemistry. *Acta Biomater.* **2009**, *5*, 2311–2321. [[CrossRef](#)]
73. Rupp, F.; Scheideler, L.; Olshanska, N.; de Wild, M.; Wieland, M.; Geis-Gerstorfer, J. Enhancing surface free energy and hydrophilicity through chemical modification of microstructured titanium implant surfaces. *J. Biomed. Mater. Res. Part A* **2006**, *76A*, 323–334. [[CrossRef](#)] [[PubMed](#)]
74. Applerot, G.; Lipovsky, A.; Dror, R.; Perkas, N.; Nitzan, Y.; Lubart, R.; Gedanken, A. Enhanced Antibacterial Activity of Nanocrystalline ZnO Due to Increased ROS-Mediated Cell Injury. *Adv. Funct. Mater.* **2009**, *19*, 842–852. [[CrossRef](#)]
75. Storrie, H.; Stupp, S.I. Cellular response to zinc-containing organoapatite: An in vitro study of proliferation, alkaline phosphatase activity and biomineralization. *Biomaterials* **2005**, *26*, 5492–5499. [[CrossRef](#)] [[PubMed](#)]

**Disclaimer/Publisher’s Note:** The statements, opinions and data contained in all publications are solely those of the individual author(s) and contributor(s) and not of MDPI and/or the editor(s). MDPI and/or the editor(s) disclaim responsibility for any injury to people or property resulting from any ideas, methods, instructions or products referred to in the content.